Smart Structures and Systems, *Vol. 36, No. 2 (2025) 111-122*
https://doi.org/10.12989/sss.2025.36.2.111

Novel multimodal shunt circuit architecture for simultaneous subsonic flutter control and energy scavenging

Suleiman Ibrahim Mohammad[*1,2], Asokan Vasudevan [3,4], A'kif Alfugara [5], Mohammed Rauf Abdullah [6], Habib Kraiem [7], Yasser Alashker [8,9] and Murat Yaylacı [10,11]

[1] *Electronic Marketing and Social Media, Economic and Administrative Sciences, Zarqa University, Jordan*
[2] *Research follower, INTI International University, 71800 Negeri Sembilan, Malaysia*
[3] *Faculty of Business and Communications, INTI International University, 71800 Negeri Sembilan, Malaysia*
[4] *Shinawatra University, 99 Moo 10, Bangtoey, Samkhok, Pathum Thani 12160, Thailand*
[5] *Independent Researcher*
[6] *Department of Construction and Project Management, College of Engineering, Alnoor University, Mosul, Iraq*
[7] *Center for Scientific Research and Entrepreneurship, Northern Border University, Arar 73213, Saudi Arabia*
[8] *Department of Civil Engineering, College of Engineering, King Khalid University, PO Box 394, Abha 61411, Kingdom of Saudi Arabia*
[9] *Center for Engineering and Technology Innovations, King Khalid University, Abha 61421, Saudi Arabia*
[10] *Department of Civil Engineering, Recep Tayyip Erdogan University, 53100, Rize, Turkey*
[11] *Turgut Kıran Maritime Faculty, Recep Tayyip Erdogan University, 53900, Rize, Turkey*

(*Received March 12, 2025, Revised August 8, 2025, Accepted August 14, 2025*)

Abstract. This paper discusses a new multimodal shunt circuit architecture for simultaneous subsonic flutter control and energy scavenging for aerospace, mechanical, etc. The system includes a finite element electromechanical modeling approach to investigate a multi-layer composite plate with an embedded piezoelectric. We construct a resonant shunt circuit in parallel, utilizing a parallel shunt circuit with two modes operating in parallel to dampen unwanted vibrations. This architecture allows us to extract energy from the plate and damp unwanted vibrations, which ideally relates to subsonic flutter. The finite element model accounts for the structural dynamics of the plate and the piezoelectric dynamics, but also allows us to tune the energy dissipation and scavenging process. The resonant shunt circuit is tuned to specific frequencies and therefore aids the dissipation of energy from the vibration modes and dampens any unwanted oscillation. The study provides a comprehensive description of tuning the shunt circuit and describes the performance of the system under varying flow conditions. To describe how the piezoelectric plate will be subjected to airflow, a diagram was included that provides a good opportunity to visualize part of this system's mechanics. As shown, the presented results indicate that this implementable structure represents innovative advancements in flutter control and energy harvesting and is an exciting opportunity for further work on adaptive structures within aerospace, automotive, and energy-efficient industries.

Keywords: composite plate; energy scavenging; finite element modelling; multimodal shunt circuit; piezoelectric component; subsonic flutter control

1. Introduction

Piezoelectric structures or piezoelectric materials are materials that produce electrical charges in response to mechanical stresses applied to the materials (De Marqui Jr *et al*. 2011, Arshid *et al*. 2023a). These piezoelectric structures have become more and more prevalent in engineering because of their ability to convert mechanical energy to electrical energy and electrical energy to mechanical energy (Leão *et al*. 2016, Li *et al*. 2025). These structures have many applications, such as power, sensors, actuators, and energy harvesting devices (Asadi and Farsadi 2020). Engineers from many different fields have exploited and continue to use piezoelectric material to create energy-efficient systems that are compact and responsive in areas like the aerospace, automotive, and robotics industries (Beni and Beni 2022). In the area of structural health monitoring, a piezoelectric sensor can detect even the smallest changes in pressure, strain, or vibrations so engineers can assess a large infrastructure problem (Al-Furjan *et al*. 2022). In precision control situations where the motion must be small and accurate, using piezoelectric structures can provide significant benefits if creating a device that relies on the precision and quickness (Alshenawy *et al*. 2022). Piezoelectric structures do not rely on external energy sources, making them ideal for devices in remote, portable, or free-moving situations (Alshenawy *et al*. 2023). Piezoelectric materials are usually lightweight structures that can be very durable and act in extreme environmental conditions, making them appealing for applications involving space exploration and medical devices (Hagood and Von Flotow 1991). For example, when dealing with energy harvesting from vibrations, piezoelectric structures can be used to generate the

*Corresponding author, Ph.D.,
E-mail: dr_sliman@yahoo.com

ISSN: 1738-1584 (Print), 1738-1991 (Online)

appropriate electrical energy to power small electronic or sensor devices (Wu 1998). This decreases the need for batteries and other conventional energy sources, providing a sustainable alternative (Wang *et al*. 2025). With an increase in demand for more intelligent, self-sustaining systems, piezoelectric materials will be a major contributor to the next wave of technology (Abad and Rouzegar 2019). Engineers will be able to leverage this property of piezoelectricity to further expand the possibilities of design for new energy-efficient devices (Arefi and Bidgoli 2019), since the structures left in this study will contribute to an updated and novel approach to engineering practices, increasing the improvement of sustainability of numerous fields of engineering (Arshid *et al*. 2023b).

Energy harvesting in structures is becoming more important in consideration of the renewed emphasis on sustainable, autonomous systems. Essentially, energy harvesting is the ability to capture and store small amounts of energy from ambient resources (such as vibration, light, heat, or wind), and ultimately convert and use this energy as power (Dias *et al*. 2015, Cao *et al*. 2022, Naranjo-Pérez *et al*. 2024). Energy harvesting offers an alternative to dependence on external power grids when implemented in buildings and other infrastructures; thus, it serves more sustainable and efficient energy solution (Kameyama and Makihara 2017). Environmental impacts are minimized when energy harvesting systems are included in the built environment (Sheeraz *et al*. 2022), and this is especially beneficial when recent calls for sustainable living and inferior access to electricity are considered (Lin *et al*. 2024). Leading off from all of this, energy harvesting is also beneficial for those practicing engineering. As an increasingly common practice, engineers incorporate energy harvesting into design to create smart buildings capable of responding to their environments and managing their own power requirements (Lien and Shu 2012, Bahrami and Motaei 2025). This could lead to more efficient lighting, climate control, and overall energy consumption in buildings (Ma *et al*. 2021). Energy harvesting technologies, like piezoelectric devices, thermoelectric generators, and photovoltaic cells, enable structures to generate energy from motion, temperature differences, and sunlight, respectively (Mangalasseri *et al*. 2023). Piezoelectric materials, for example, convert vibrations or mechanical stress into electrical energy, which can be used to power sensors or other small devices embedded in the structure (Ravanbod and Ebrahimi-Nejad 2024). This may improve lighting, climate control, and energy use in buildings (Ma *et al*. 2021). Energy harvesting technologies, such as piezoelectric materials, thermoelectric generators, and photovoltaic cells allow buildings to generate energy using motion, temperature differences and light, respectively (Mangalasseri *et al*. 2023). Piezoelectric materials convert the mechanical stress or vibrations of the building into electrical energy, enough to power wire sensors or other small devices embedded in the structure (Ravanbod and Ebrahimi-Nejad 2024).

Stability analysis for structures (buildings, bridges, etc.) is important in engineering to determine if the components will adequately support loads and forces without collapsing or experiencing structural failure (Rabczuk *et al*. 2007). This analysis is used to find potential failure modes such as buckling, overall structural instability, and excessive deflection that might compromise the overall integrity of the structure (Rabczuk *et al*. 2019). The stability analysis is utilized when determining material behavior for a structure under different loads, including dead loads, live loads, wind loads, and/or seismic forces (Bai *et al*. 2024). This analysis is even more relevant to tall buildings or bridges, or other large structures, which may have their own unique stability challenges, requiring one to realize that stability (under full and partial loading conditions) is important to ensure safety. By conducting a stability analysis, engineers can ensure they are meeting safety standards and building codes, and determine other factors like allowable deflections. Also, depending on the magnitude of the loads, an analysis of a structure can help fortify design materials used, allowing for the safe and economical use of materials as well. Stability analysis is important in the preliminary stages of a design process to evaluate how a structure is supposed to behave in real situations to aid the designer in addressing changes to the original design. In a dynamic environment, like areas that experience earthquakes and heavy winds, stability analysis is especially necessary for analyzing the effects of these forces on the expected behavior of the structure, it may even facilitate the design of new material and construction methods that enhance stability over time (Zare *et al*. 2020). Stability analysis mainly considers long-term stability of a structure to reduce maintenance costs, which in turn may improve safety (Foroutan *et al*. 2022).

This work presents a novel multimodal shunt circuit design that addresses subsonic flutter control and energy scavenging in structural systems simultaneously. The system is constructed using a finite element electro-mechanical model to study a composite plate with a piezoelectric element fully embedded within. The multimodal shunt is based on a resonant shunt circuit that is configured in parallel to target and dampen two vibration modes separately. The parallel shunt circuit allows energy harvesting at multiple frequencies while concurrently helping to control vibration. This places the design in a category of innovative and advanced systems with applications in aerospace, automotive, and multiscale energy harvesting technologies. The model captured electromechanical coupling between the dynamics of the plate and the piezoelectric mechanics. The electro-mechanical model allows for a more comprehensive understanding of the system's energy harvesting perfor-mance when applied under varying flow conditions. An overall diagram of the piezoelectric plate subjected to airflow is given. The results find that this proposed multimodal shunt circuit design achieves better flutter control, while also supporting improved energy harvesting, and presents a compelling example of an adaptive, self-sustaining system. The contributions of this study can be segmented into four areas: 1. The multi-modal shunt circuit architecture proposed successfully combines subsonic flutter control and energy harvesting into a single device for dynamic structural systems; thus, this work delivers a dual-functional capability. 2. To examine the electromechanical coupling between the piezoelectric element and multi-layered composite plate, finite element modeling was

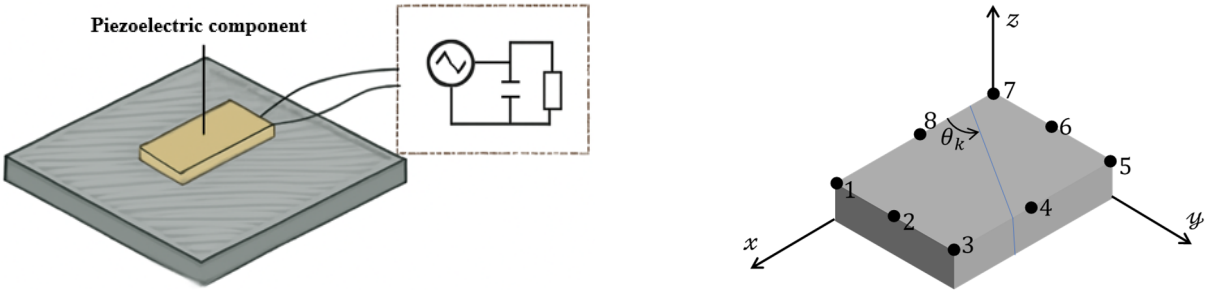

(a) Architecture design of the mentioned structure (b) Mathematical modeling

Fig. 1 A diagram showing a multi-layered structure with a piezoelectric component embedded in a composite plate

employed to obtain an accurate representation of the system through simulation for performance prediction. 3. The work features a design that allows for a parallel resonant shunt circuit to operate at multiple frequencies to increase the effectiveness of damping against several vibrational modes are used for improving energy harvesting and vibration suppression for a range of operational conditions. 4. This study represented the effects of air flow into the modeling scheme so that the live system can also adapt to changes in external conditions. This is significant for applying the findings of this research to real-world settings, specifically, aerospace environments where airflow characteristics are paramount.

2. Finite element electromechanical modeling

The use of finite element electromechanical modeling combines finite element analysis (FEA) with electromechanical systems, irrespective of the degree of coupling in order to obtain a digital representation in which the forces applied result from mechanical and electrical conditions. The mechanical portion of a system (e.g., plates or beams) is simulated using the same methods as with standard techniques of FEA to obtain stress, strain and displacement. The electrical portion of the system (e.g., any piezoelectric or capacitive materials) is then modeled to simulate properties, such as charge distribution, electric field, and energy conversion processes. Certain finite element models contain both mechanical and electromechanical aspects and clocks under both dynamic load conditions to allow for accurate predictions of system behavior with regards to dynamic stimuli (Kheirikhah *et al*. 2012). Finite element modeling of this nature benefits the researcher or designer who in these cases are addressing problems related to: designing energy harvesting or actuation devices, vibration control, and smart material structures for applications in aviation or mechanical engineering. For a further discussion on modeling electromechanical systems according to conservative and higher order shear deformation theories (HSDT), see (Kheirikhah *et al*. 2012).

$$\mathfrak{A}(a,b,z,t) = \boldsymbol{a}(z)\boldsymbol{n}(a,b)\mathfrak{A}_{\mathbf{e}}(t), \tag{1a}$$

$$\begin{aligned}\boldsymbol{\mathcal{E}}(a,b,z,t) &= \boldsymbol{d}(z)\boldsymbol{n}(a,b)\mathfrak{A}_{\mathbf{e}}(a,b,t)\\ &= \boldsymbol{\mathcal{b}}(a,b,z)\mathfrak{A}_{\mathbf{e}}(t).\end{aligned} \tag{1b}$$

The vector $\mathfrak{A}(a,b,z,t) = [\mathbb{u}(a,b,z,t)\mathbb{v}(a,b,z,t)\ \mathbb{w}(a,b,z,t)]^{\mathrm{T}}$ represents the displacement components in the x, y, and z directions. The function $\boldsymbol{n}(a,b)$ corresponds to the shape functions in the local coordinate system, where a and b are defined within the range $-1 \le b \le 1$ and $-1 \le a \le 1$, respectively. The vector $\mathfrak{A}_e(t) = \left[u_{0_i}\ v_{0_i}\ w_{0_i}\ u_{1_i}\ v_{1_i}\ u_{2_i}\ v_{2_i}\ u_{3_i}\ v_{3_i}\right]^{\mathrm{T}}$ (for $i = 1, \ldots, 8$) describes the nodal displacements. Lastly, $\boldsymbol{d}(z)$ represents the matrix of differential operators. Fig. 1 depicts a composite plate with a piezoelectric device installed in a multi-layered configuration. The figure shows a coordinate system indicating that the problem is likely three-dimensional with an x, y, z axis. The numbers 1-8 are primary points on the structure, probably denoting indexed locations or features in the composite material, which are also marked on the outside edge of the plate. It appears that the structure is being reviewed with respect to angles, defined by the vector θ_k in the figure, which probably indicates a particular angle of analysis within the configuration or force or strain orientation or application. A piezoelectric device usually generates electrical charge output in response to mechanical stress, which seems to be the goal of the structure they are analyzing in Fig. 1. The figure serves as a visualization tool to assist understanding the mechanical or electrical response of the embedded piezoelectric element, in the right context. Multi-layered structures like this one are important to design and analysis of materials properties; specifically, whether the mechanical strain, electrical fields, or even coupled interactions in material systems can be achieved, and how that can be optimized for interaction of the piezoelectric material with the layers surrounding it, to be applied in any number of applications possibly including sensors, actuators, or energy harvesting devices/systems.

The relationships between deformation and displacement matrices are outlined as follows

$$\boldsymbol{m}_{uu}^{e} = \sum_{k=1}^{n} \int_{z=z_k}^{z=z_{k+1}} \int_{b=-1}^{b=1} \int_{a=-1}^{a=1} \rho_k \boldsymbol{n}(a,b)^{\mathrm{T}} \boldsymbol{a}(z)^{\mathrm{T}} \boldsymbol{a}(z) \boldsymbol{n}(a,b) \det(\mathbf{J}) dadbdz, \tag{2a}$$

$$\boldsymbol{k}_{uu}^{e} = \sum_{k=1}^{n} \int_{z=z_k}^{z=z_{k+1}} \int_{b=-1}^{b=1} \int_{a=-1}^{a=1} \boldsymbol{b}(a,b,z)^{T} \mathbf{T} \boldsymbol{c} \mathbf{T}^{\mathrm{T}} \boldsymbol{b}(a,b,z) \det(\mathbf{J}) dadbdz. \tag{2b}$$

In this context, $\boldsymbol{c}$ denotes the orthotropic elasticity matrix for the kth layer, aligned with its principal material directions. $\mathbf{T}$ represents the transformation matrix used to modify the mechanical properties of each layer. The electric potential in the kth layer is derived by interpolating interface values with the shape functions $\boldsymbol{\mathcal{L}}(\boldsymbol{z})$. The electric field is then described as outlined in Ref. (Tiersten 2013).

$$\mathbf{E}_{(k)}(a,b,z,t) = -\nabla \mathfrak{H}_{(k)}(a,b,z,t) = -\nabla \boldsymbol{n}_{\mathfrak{H}}(a,b,z) \boldsymbol{\mathfrak{H}}_{\boldsymbol{e}}(t) = -\boldsymbol{b}_{\mathfrak{H}}(a,b,z) \boldsymbol{\mathfrak{H}}_{\boldsymbol{e}}(t). \tag{3}$$

In this formulation, $\boldsymbol{n}_{\mathfrak{H}}$ is the shape function matrix in the local coordinate system. The electromechanical strain energy is derived using linear piezoelectric theory (Tiersten 2013) and expressed as shown in Refs. (Al-Furjan *et al*. 2020, Yang *et al*. 2024, Wang *et al*. 2025).

$$U = \int_{V} (\boldsymbol{\mathcal{E}}^{\mathrm{T}} \boldsymbol{\sigma} - \mathbf{E}^{\mathrm{T}} \boldsymbol{d}) \, dV. \tag{4}$$

Here, $\boldsymbol{d}$ is the electric displacement vector, and $\boldsymbol{\sigma}$ is the mechanical stress tensor. Using the strain formulations in Eqs. (3) and (1b), the core stiffness matrices for electromechanical behavior are derived as shown below.

$$\begin{bmatrix} \boldsymbol{m}_{uu} & 0 \\ 0 & 0 \end{bmatrix} \begin{Bmatrix} \ddot{\mathfrak{U}}_g(t) \\ \ddot{\mathfrak{H}}_g(t) \end{Bmatrix} + \begin{bmatrix} \boldsymbol{k}_{uu} & \boldsymbol{k}_{uv} \\ \boldsymbol{k}_{vu} & \boldsymbol{k}_{vv} \end{bmatrix} \begin{Bmatrix} \mathfrak{U}_g(t) \\ \mathfrak{H}_g(t) \end{Bmatrix} = \begin{Bmatrix} \boldsymbol{\mathcal{F}}_g(t) \\ \boldsymbol{\mathcal{Q}}_g(t) \end{Bmatrix}. \tag{5}$$

In this context, **e** is the electric permittivity, and $\boldsymbol{\chi}^{e}$ is the dielectric constant matrix, both initially defined in the principal directions of each layer and transformed using matrices $\boldsymbol{\mathcal{F}}$ and $\boldsymbol{\mathcal{Q}}$. The Jacobian determinant, **det(J)**, governs the transformation from the local to global coordinate systems, and the motion equations are derived via finite element methods to model the coupled electromechanical response.

$$\left[\underbrace{\boldsymbol{k}_{uu} - \boldsymbol{k}_{uv} \left(\boldsymbol{k}_{vv} - \frac{1}{i\omega} \mathbf{Z}^{-1}(\omega) \right)^{-1} \boldsymbol{k}_{uv}^{\mathrm{T}}}_{\boldsymbol{k}_T} - \omega^2 \boldsymbol{m}_{uu} \right] \mathfrak{U}(\omega) = \boldsymbol{\mathcal{F}}(\omega). \tag{6}$$

The electromechanical coupling is analyzed in the frequency domain, considering the frequency-dependent electrical impedance $\mathbf{Z}(\omega)$ of the external circuit. After system assembly, the coupled model in the frequency domain is expressed as follows.

$$\left[\underbrace{\boldsymbol{k}_{uu} - \boldsymbol{k}_{uv} \left(\boldsymbol{k}_{vv} - \frac{1}{i\omega} \mathbf{Z}^{-1}(\omega) \right)^{-1} \boldsymbol{k}_{uv}^{\mathrm{T}}}_{\boldsymbol{k}_T} - \omega^2 \boldsymbol{m}_{uu} \right] \mathfrak{U}(\omega) = \boldsymbol{\mathcal{F}}(\omega). \tag{7}$$

Fig. 2 shows a resonant shunt circuit designed in parallel to dampen 2 modes of vibration. There are many other elements; capacitors, resistors, and inductors connected for a range of controlling for the dissipation of energy. The main components consist of the piezoelectric capacitor $\mathbb{c}_{pzt}$, resonant capacitor $\bar{\mathbb{c}}_1$ capacitor, inductive resistive networks labelled $\mathcal{T}_1$, and $\mathcal{T}_2'$ as well as resistive components $\mathbb{r}_1$ and $\mathbb{r}_2'$. This type of configuration works by connecting energy dissipation through a resonant circuit tuned to the natural vibration frequencies of the modes of interest. Each resonant network $\mathcal{T}_1$, and $\mathcal{T}_2'$ act to absorb energy from specific modes of vibration in order to dampen an undesired mode. It is the resistive components $\mathbb{r}_1$ and $\mathbb{r}_2'$ that provide the energy dissipation, while the inductive components $\mathcal{T}_1$, and $\mathcal{T}_2'$ ensure the circuits are in a resonance condition for damping to occur. This type of circuitry is ideal for situations when damping is required, such as vibration sensitive applications, or where both

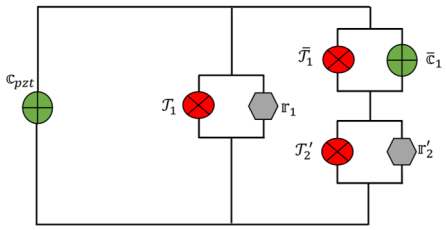

Fig. 2 A resonant shunt circuit configured in parallel, intended to dampen two vibration modes

vibration suppression and energy harvesting is required. By tuning the circuit to the resonant frequency of the modes of vibration, this type of electrical circuitry would enhance overall performance for the purposes of controlling vibrations and harvesting energy.

3. Parallel shunt circuit operating at multiple frequencies

As shown in Fig. 2, the multi-resonant parallel shunt circuit allows independent control of subsonic flutter and structural vibrations. It features multiple branches, each tuned to specific dynamic modes, focusing on the first two modes related to flutter initiation. This configuration, introduced in Ref. (Wu 1998), provides effective control while minimizing blocking elements, given the mode frequencies meet the ω_1 criterion.

$$Z(\omega) = \frac{\mathbb{r}_1 \mathcal{T}_1 \omega \left[\frac{\overline{\mathcal{T}}_1}{\overline{\mathbb{c}}_1\left(\overline{\mathcal{T}}_1 i\omega - \frac{i}{\overline{\mathbb{c}}_1 \omega}\right)} + \frac{\mathcal{T}_2' \mathbb{r}_2' i\omega}{\mathbb{r}_2' + \mathcal{T}_2' i\omega}\right] i}{(\mathbb{r}_1 + \mathcal{T}_1 i\omega)\left[\frac{\overline{\mathcal{T}}_1}{\overline{\mathbb{c}}_1\left(\overline{\mathcal{T}}_1 i\omega - \frac{i}{\overline{\mathbb{c}}_1 \omega}\right)} + \frac{\mathcal{T}_1 \mathbb{r}_1 i\omega}{\mathbb{r}_1 + \mathcal{T}_1 i\omega} + \frac{\mathcal{T}_2' \mathbb{r}_2' i\omega}{\mathbb{r}_2' + \mathcal{T}_2' i\omega}\right]}. \quad (8)$$

In Eq. (8), $\mathbb{r}_i = \left[\sqrt{2}\mathbb{c}_{pzt}\omega_i \boldsymbol{k}_{31}\right]^{-1}$, $\mathcal{T}_i = \left[\mathbb{c}_{pzt}\omega_i^2(1 - 0.5\boldsymbol{k}_{31}^2)\right]^{-1}$, and $\mathbb{c}_{pzt} = \boldsymbol{k}_{vv} - \boldsymbol{k}_{uv}^{\mathrm{T}}(\boldsymbol{k}_{vv})^{-1}\boldsymbol{k}_{uv}$ ($i = 1,2$). Also, have

$$\mathbb{r}_2' = \frac{\mathbb{r}_1 \mathbb{r}_2}{\mathbb{r}_1 - \mathbb{r}_2}, \quad (9a)$$

$$\mathcal{T}_2' = \frac{\mathcal{T}_1\mathcal{T}_2 + \mathcal{T}_2\overline{\mathcal{T}}_1 - \mathcal{T}_1\overline{\mathcal{T}}_1 - \omega_2^2\mathcal{T}_1\mathcal{T}_2\overline{\mathcal{T}}_1\overline{\mathbb{c}}_1}{(\mathcal{T}_1 - \mathcal{T}_2)\left(1 - \omega_2^2\overline{\mathcal{T}}_1\overline{\mathbb{c}}_1\right)}. \quad (9b)$$

4. Aeroelectromechanical model

The dimensionless mean induced velocity, $\overline{\mathbf{w}}_N$, is given by $\overline{\mathbf{w}}_N = \boldsymbol{a}\boldsymbol{I}\boldsymbol{c}^{-1}\Delta\mathbf{c}_\mathbf{p}$, where $\boldsymbol{a}\boldsymbol{I}\boldsymbol{c}$ is the aerodynamic influence coefficient matrix and $\Delta\mathbf{c}_\mathbf{p}$ is the vector of nondimensional pressure differences. Integration of the aerodynamic and structural domains is achieved by aligning their computational meshes, as shown in Fig. 3. For further details, refer to

$$\overline{\boldsymbol{m}}\ddot{\boldsymbol{q}} + \overline{\boldsymbol{k}}\boldsymbol{q} = q_\infty \boldsymbol{Q}_\mathbf{a}(ik_r)\boldsymbol{q}. \quad (10)$$

In this analytical model, $\overline{\boldsymbol{m}}$ and $\overline{\boldsymbol{k}}$ represent the modal mass and stiffness matrices, while q_∞ denotes the dynamic pressure of the free-stream flow, and $\boldsymbol{Q}_\mathbf{a}(ik_r)$ is the generalized aerodynamic matrix (GAM) dependent on the reduced frequency $k_r = \omega b/V$. To predict flutter onset, the coupled aeroelastic equations are solved through eigenvalue analysis, with the PK method offering higher accuracy than the classical K method due to its assumption of dominant harmonic oscillations.

$$\left[p^2\overline{\boldsymbol{m}} - \frac{1}{2}\frac{b}{k_r}\rho V\Im(\boldsymbol{Q}_\mathbf{a})p + \overline{\boldsymbol{k}} - \frac{1}{2}\rho V^2\Re(\boldsymbol{Q}_\mathbf{a})\right]\boldsymbol{q} = \mathbf{0}. \quad (11)$$

Eq. (11) presents a state-space representation of the aeroelastic system, integrating structural dynamics, aerodynamic forces, and electromechanical interactions.

$$\boldsymbol{a} = \begin{bmatrix} \mathbf{0} & \mathbf{I} \\ -\overline{\boldsymbol{m}}^{-1}\left(\overline{\boldsymbol{k}} - \frac{1}{2}\rho V^2\Re(\boldsymbol{Q}_\mathbf{a})\right) & \overline{\boldsymbol{m}}^{-1}\left(\frac{1}{2}\frac{b}{k_r}\rho V\Im(\boldsymbol{Q}_\mathbf{a})\right) \end{bmatrix}. \quad (12)$$

4.1 Vibration energy harvesting

For aerodynamic loading $\boldsymbol{Q}_{\mathbf{a}\mathcal{F}}$ and electrical voltage per unit force, the expressions are as follows

$$\frac{\boldsymbol{\varphi}_0(\omega)}{\boldsymbol{\mathcal{F}}_0(\omega)} = \left[\boldsymbol{k}_{vu}\boldsymbol{a}_a^{-1}\boldsymbol{k}_{uv} - \boldsymbol{k}_{vv} + \frac{\mathbf{Z}^{-1}(\omega)}{i\omega}\right]^{-1}\boldsymbol{k}_{uv}\boldsymbol{a}_a^{-1} = \mathbf{V}_0(\omega). \quad (13)$$

where $\boldsymbol{a}_a = \left[\boldsymbol{k}_{uu} - \frac{\rho V^2}{2}\Re(\boldsymbol{Q}_{\mathbf{a}_F}) - i\omega\frac{\rho V}{2}\Im(\boldsymbol{Q}_{\mathbf{a}_F}) - \omega^2\boldsymbol{m}_{uu}\right]$. Also, have

$$\mathbf{P}_0(\omega) = \frac{\mathbf{V}_0(\omega)^2}{2|Z(\omega)|}. \quad (14)$$

5. Computational modeling

The schematic shown in Fig. 3 represents a piezoelectric plate with specified dimensions with a thickness of 1 mm, a width of 160 mm, and a length of :320 mm. This was used as a physical model of the system in which the multimodal shunt-circuit is implemented. The structure is a rectangular block form which has dimensions of 160 mm by 320 mm in the plane of the material and a height of only $1\ mm$ makes this a thin flat object. The axes are labeled x, y, and z with the 'z' axis located in the vertical position (position of motion or vibration). The arrows labeled 'y' show the direction of vibration describing that the system aims to capture vibrational energy in the z direction, typically the vertical direction. This model might represent a thin flexible

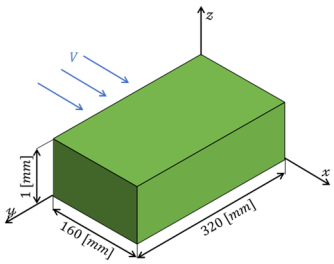

Fig. 3 A diagram illustrating the configuration of the piezoelectric plate subjected to airflow

plate or panel or a thin plate material often used in energy-harvesting and/or vibration juddering contexts. The dimensions indicate that this may be part of a system related to aerospace or automotive applications, with the significant control of flutter and vibrations to maintain performance and safety. The resonant shunt circuit was implemented in this model to harvest energy from the vibrational modes, while simultaneously suppressing vibrations. Hence this design can work in applications that require the suppression of vibrations with energy recovery. This exercise demonstrates a clear real-world application of multimodal damping and energy scavenging.

Ref. (Su *et al*. 2018) provides a summary of the mechanical, electromechanical, and electrical properties of the PZT-5H piezoelectric material used in this study. Additionally, the material properties of the composite layers are outlined in Ref. (Kulkarni and Kapuria 2008).

5.1 Verification of the results

Table 1 includes a comparison of the dimensionless fundamental (transverse) natural frequencies, for both isotropic thick and moderately thick plates, focusing on different method to calculate the frequencies. The results discuss the various dimensionless natural frequencies for the ratio a/h (a is the plate length and h is the thickness). The comparisons used Exact 3D analysis, Quasi-3D analysis, and our method with $\boldsymbol{\varepsilon_{zz}}$ = 0, where $\boldsymbol{\varepsilon_{zz}}$ refers to the normal stiffness value, accounting for normal stress in z-direction. Normal stress in the z-direction represents stress of the out-of-plane direction, and can have serious impact on the global response of the plate, especially when the plate is thick or moderately thick. The Exact 3D analysis (cited as (Jin *et al*. 2014)) is taken as solution of reference, and this represents the results from the Quasi-3D method and our current method. The results for $a/h = 2$ indicate that the Exact 3D method produces a frequency of 1.8470; the Quasi-3D method predicts a frequency of 1.8528; and the present method, which includes $\boldsymbol{\varepsilon_{zz}}$, produces a frequency of 1.8510. When a/h increases (i.e., at $a/h = 10$) the natural frequencies converge (see last rows where the natural frequency is 0.1135 for all methods). This also indicates that the influence of $\boldsymbol{\varepsilon_{zz}}$lessens as the plate thickens. The present method provides a very accurate approximation of the Exact 3D solution by including the normal stress along the z-direction; therefore, the present method has demonstrated the ability to model the complexity in vibrational

Table 1 The dimensionless fundamental (transverse) natural frequency of isotropic thick and moderately thick plates is provided, with the dimensionless parameters detailed in Ref. (Jin *et al*. 2014)

a/h		
2	Exact (3D) (Jin *et al*. 2014)	1.8470
	Quasi-3D (Farzam-Rad *et al*. 2017)	1.8528
	Present ($\boldsymbol{\varepsilon_{zz}} \neq 0$)	1.8510
5	Exact (3D) (Jin *et al*. 2014)	0.4169
	Quasi-3D (Farzam-Rad *et al*. 2017)	0.4170
	Present ($\boldsymbol{\varepsilon_{zz}} \neq 0$)	0.4169
10	Exact (3D) (Jin *et al*. 2014)	0.1135
	Quasi-3D (Farzam-Rad *et al*. 2017)	0.1136
	Present ($\boldsymbol{\varepsilon_{zz}} \neq 0$)	0.1135

characteristics of thick and moderately thick plates, while also decreasing the number of computations. Overall, the table suggests that in modeling thick plates it is imperative to include normal stress effects especially when comparing computational methods which utilize accuracy and efficiency.

The multi-objective robust optimization problem, with the circuit parameters as the design variables, is formulated as follows

$$r_1 = -V_f, \quad r_2 = -P_{0_f}, \quad s_1 = \frac{\sigma_1}{\mu_1}, \quad s_2 = \frac{\sigma_2}{\mu_2}. \tag{15}$$

5.2 Results and discussion

Fig. 4 shows the distribution of SEs experienced by a composite structure that was excited in torsional mode. The matrix format indicates SEs across a 12×12 grid. Each element of the grid refers to the SE at that specific location in the structure as denoted by the row and column number. Color grading was used (from yellow to purple), the where the values of SE increases from low in yellow to high in purple. The locations with high values of SE were conducted in certain areas of the structure, namely; 143.68 located at (11,12). Understanding the SE distribution will help further our knowledge on how the multimodal shunt circuit architecture works to interact with the structure subjected to vibration. Particularly, the locations with the highest values of SE will provide the best approximate locations for the piezoelements embedded in the structure as these locations are where the most amount of energy can be harvested from the structure, and the best vibrations will be damped. Analyzing the SE distribution allows us to evaluate the degree to which the resonant shunt circuit is fully insulative of all of the energy absorbed and dissipated from the mass and structure overall (more specifically, where the intensity of the torsional mode is highest). The SE distribution profile is extremely valuable when attempting to optimize the performance of the circuit for controlling subsonic flutter in conjunction with maximizing energy scavenging. The SE distribution and finite element model characterizations provide additional information about the

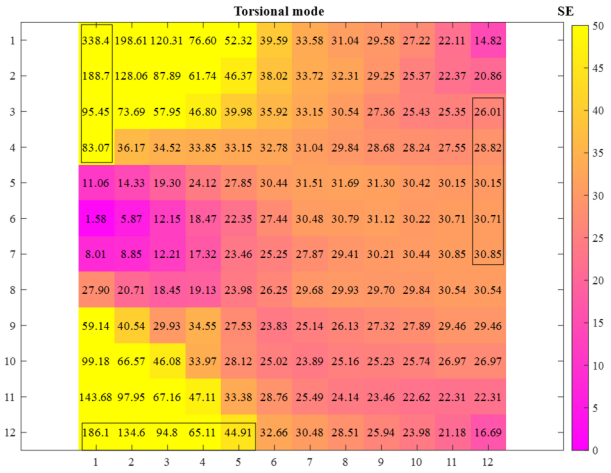

Fig. 4 The distribution of strain energy across a composite structure subjected to a torsional mode of vibration

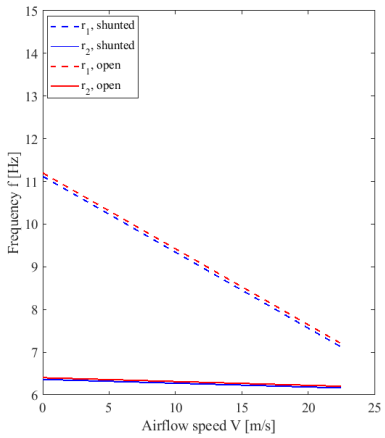

Fig. 5 The relationship between the natural frequency and airflow speed for two distinct modes of vibration, r_1 and r_2, under both shunted and open circuit conditions

system when subject to dynamic variation where only the resonant shunt circuit is engaged.

Fig. 5 shows the relationship between natural frequency and airflow speed (V) for two different modes of vibration, r_1 and r_2 in shunted and open circuit. The shapes of the curves indicate that as airflow speed increases the natural frequency of both modes decreases. There is a pronounced decrease in frequency under open circuit conditions (red lines) compared to shunted conditions (blue lines). This indicates that the response in the shunted system is better at providing damping of vibrations over a large range of airflow speeds. The two modes r_1 and $r_2$are both considered separately, with the difference in frequency response indicating the system is operating in modes of vibration. The shift in the frequencies with airflow conditions is relevant to energy harvesting and flutter control respectively for aerodynamic systems, since this behavior indicates a dynamic response of the system to the external airflow which will impact the energy conversion efficiency and maximization, and controlling undesirable vibration behaviors like flutter. These findings will

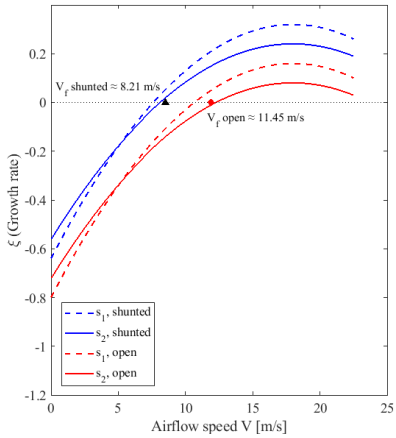

Fig. 6 The relationship between growth rate and airflow speed for the system, exploring the vibration modes under both shunted and open circuit conditions

contribute to the design process of piezoelectric-based energy harvesting systems for aerospace considerations.

Fig. 6 shows the relationship between growth rate and airflow speed for the system, exploring the vibration modes under both shunted and open circuit conditions. The growth rate is an important indicator of the system's stability and demonstrates the transition from stable to unstable behavior as airflow speeds increase. The growth rate, shown in Fig. 6 initially remains negative, which indicates a stable condition at low speeds, then as airflow speeds are increased, the growth rate begins to increase and eventually becomes positive indicating the onset of flutter. Two critical points are indicated showing the flutter speed for the shunted and the open condition respectively. The critical points show the flow speeds which the system starts to move into the instable flutter regime. The open condition shows a greater increase in growth rates and as such, it would appear that the shunted configuration of the system does a better job of suppressing the flutter. Overall results are critical to understanding the systems stability in different airflow conditions and provide a better insight into how to design systems which must balance flutter control and energy harvesting applications, particularly in aerodynamics and energy harvesting applications.

Fig. 7 presents harvested power (W) plotted against flutter speed (m/s). The figure provides evidence of the relationship between flutter speed and harvested power. There is a clear trend of increasing harvest power with increasing flutter speed. Furthermore, the system is clearly capable of harvesting energy even at higher flutter speeds. At low flutter speeds, harvested power was low, but once the system was in the flutter regime, the harvested power subsequently increased significantly. This figure also includes the Pareto front, represented by the red line, which demonstrates the trade-off between harvested power and flutter speed, identifying the optimal conditions for energy harvesting. Each design point (blue dots) represents the modelling configurations for the system with various combinations of harvested power and flutter speed. This figure exemplifies the necessary trade-off of having high energy characteristics while not allowing too much flutter,

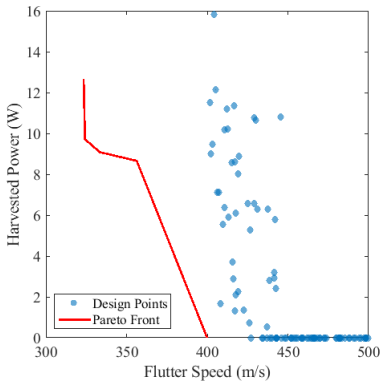

Fig. 7 The relationship between harvested power (W) and flutter speed (m/s) for the system

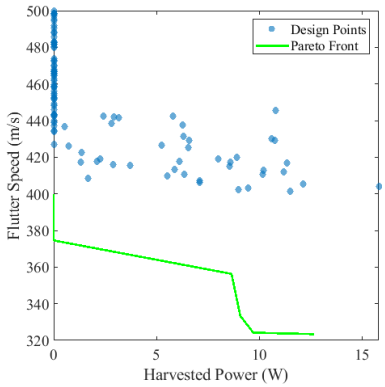

Fig. 8 The relationship between flutter speed and harvested power, with the aim of optimizing both variables for efficient operation

which would lead to an unstable system. The results have demonstrated that not only is it necessary to optimize the individual system to maximize energy harvesting, but it is also equally important to fine-tune the control of flutter which increases our understanding of piezoelectric energy harvesting systems in subsonic flows. These results will be beneficial for the field of adaptive structures in aerospace and mechanical engineering applications.

Fig. 8 depicts the relationship between flutter speed and harvested power while trying to maximize both traits for effective operation. The contour line in the figure shows that as flutter speeds increased, harvested power also increased, then plateaued, indicating diminishing returns at higher flutter speeds. The green line indicates the Pareto front, which denotes the best tradeoff between flutter speed and harvested power; this aspect can aid designs, or better designs, while incorporating flutter suppression for energy harvesting. The blue dots indicate the design points for different operational options of the system; they also represent as a visual depiction of changing system designs parameters, and what it does to the produced loads in our case, collecting power. Keeping in mind design goals to maximize energy harvesting while effectively suppressing flutter to avoid excessive flutter that could create a system failure was part of the challenge. These results describe the need to balance energy harvesting and flutter suppression,

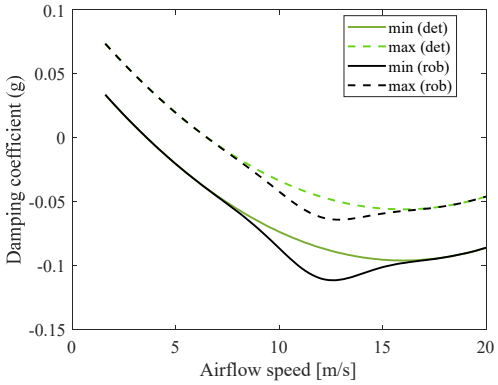

Fig. 9 The variation of the damping coefficient with airflow speed. The plot includes the minimum and maximum damping coefficients for two configurations: deterministic and robust

and may show how we could tune the aerodynamic properties of the system, or the structural properties for detrimental vibrations to improve system performance in energy harvesting applications, e.g., aerospace and mechanical systems. The information we gathered with this study may help over the design of adaptive structures that can also simultaneously harvest energy and control structural vibration or apply different dampening systems based on vibration conditions.

Fig. 9 presents the relationship between damping coefficient and airflow speed. The plots exhibit both the minimum and maximum damping coefficients for both configurations: deterministic and robust. The damping coefficient is vital to the analysis of the energy dissipation ability of any system, while vibration control and energy harvesting ability depend on the behavior of the damping coefficient (or damping ratio). For airflow speeds increasing from 0 to 20 m/s, the damping coefficient of the system increases to a maximum value of 0.041 before it begins to decrease. This is clearly shown in the differences of the damping coefficient of the structure and the corresponding power harvester and there is summary energy dissipation capacity of the system, which increases and then subsequently falls away. The differences in response between the two cases, deterministic and robust cases indicate the difference in the impact circuit parameter variabilities and the resulting forces on the damping behavior of the configuration. The robust configuration (dashed lines) damping coefficients have more variation than the deterministic case, amounting a more factored response to consistent increases in the airflow speed. The study has practical implications for energy harvesting systems as the behavior of the damping has been shown to influence vibration control meaning higher or better power generation. The results of this study could assist in the design of more efficient energy harvesting systems that require control of the system's dynamic response and energy harvesting performance as found with aerospace and mechanical systems that deal with varying fueling conditions pertaining to increased airflow conditions.

Fig. 10 depicts how damping varies with airflow speed where the variation envelope and mean response are

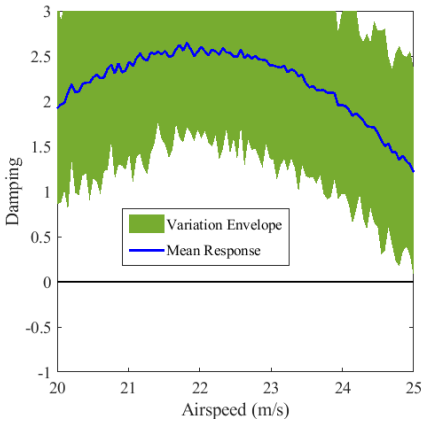

Fig. 10 The variation of damping with airflow speed, showcasing both the variation envelope and mean response

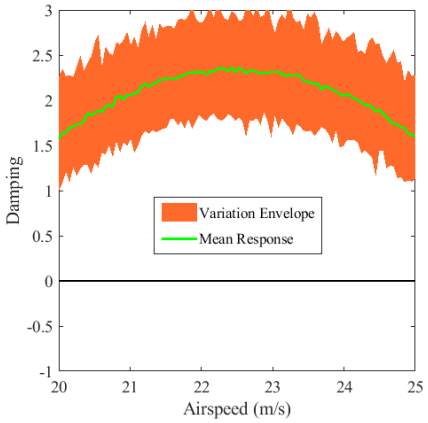

Fig. 11 Damping with respect to airflow speed, focusing on the variation envelope (orange) and the mean response (green)

evident. The variation envelope (orange) demonstrates the maximum amount of variation, or fluctuation, in damping while the mean response (green) illustrates the average damping behavior across the full speed range. As the airflow speed increases, it is clear there is a major trend of fluctuation in the damping response with a decreasing trend in the mean response. This suggests that the system can dampen vibrations; however, it is prone to variability with airflow speed, which is part of the complex dynamics of airflow-induced forces and structural response. The wide variation in damping suggests a robust control mechanism is needed to manage the performance variability to enable consistent energy harvesting and vibration control with the maximum damping reduction possible across fluctuations. The variation envelope indicates uncertainties associated with damping behavior change that need to be incorporated in a adaptive system that can accommodate fluctuation. The implications of this study are important for energy harvesting (EH) and vibration control systems for aerospace and automotive applications where flow speeds may be variable and factor into the performance expectations achievable with precise damping control for stability and energy efficiency.

In Fig. 11, we examine damping as a function of airflow speed considering the variation envelope (orange) and mean response (green). The mean response represents the average operation of the system exhibiting a dynamic damping coefficient under airflow, whereby the mean damping value reduces with a rise in airspeed. The variation envelope represents the variation around the mean response, and together the significant variation in damping reinforces the impact that aerodynamic forces have on the vibration behavior of the system. More importantly the variation provides for energy harvestable or management systems, as this will determine the energy conversion efficiency from the exciting forces will occur at different air speeds. The overall message from this figure illustrates that the system can achieve a wide variation of damping response as a result of the airflow speed, furthermore any deviation in damping will have a significant impact on stability and operation of the energy harvesting system. Variability with system damping and performance indicates that adaptive or robust approaches to control will be needed to ensure the system can react to variations in damping. The relationship between variation envelope and mean response could be indicative for the potential to optimize damping for energy harvesting and/or energy management systems subjected to variable flow conditions such as aerospace systems subjected various wind speeds. Insights like this from the project work will have use in systems engineering methods that related and produced reliable and effective systems fitted for safe operational environments.

Fig. 12 examines the system's reaction to alterations in circuit parameters as the flutter speed and power output characteristics are engaged. The plot presented examines the interplay between circuit parameter alterations and operational characteristics. In the plot, the red line depicted the change to flutter speed, while the blue line depicted the change in power output. It was determined higher circuit parameters decreased flutter speed, while power output increased, thus demonstrating a trade-off between these two significant operational characteristics. The examination of the system's changes in flutter speed and produced power indicates the need for consideration when optimizing the parameters of the system. Specifically, the outputs had an inverse relationship. Circuits required optimization on each side to achieve the necessary balance for system stability. However, it was important to note that the power outcome required consideration of each parameter's impact on the flutter characteristics. The system's engagement with each of these parameters is significant in the design of energy harvesting systems, as both vibration suppression (flutter control), and, ultimately effective energy conversion take place through circuit compliance through parameters selected. In conclusion, according to the completion of this evaluation, it will be important to focus on circuit parameters to ease the balance between stability and power production. For circuit designers, embodiment of systems in aerospace and automotive applications will ultimately benefit from derived insights investigate the extent to which circuits function to the achievement of operational objectives, in this case both, harvest energy sustainably while engaging in vibration control operations. The researcher can engage derive additional studies to optimize

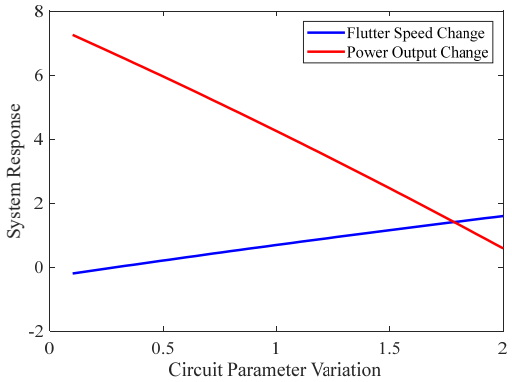

Fig. 12 The system's response to changes in circuit parameters, specifically focusing on flutter speed and power output

existing adaptive systems that include routes for energy production, while performing objectives related to vibration control; which is generally a sideline when one is engaged in energy generation optimization.

6. Conclusions

In this work, we introduced a combined multimodal shunt circuit design to simultaneously control subsonic flutter while harvesting energy. By using a finite element electromechanical modeling approach, we studied a multi-layer composite plate with an embedded piezoelectric element. This method facilitated the understanding of the complex electromechanical coupling between the structural dynamics of the plate and the piezoelectric behavior, clearly showing the feasibility of an effective vibration control and energy scavenging system. The operation of resonant shunt circuits traditionally consists of parallel circuits for each mode at their corresponding frequencies, damps two modes of vibration in a single structure, and provides more control over flutter and energy harvesting performance. We have shown that the proposed combined multimodal resonant shunt circuit has the advantages of conventional designs in that we are able to achieve vibration suppression while harvesting energy. The dual functionality feature was most suitable for applications wherein both structural health and energy efficiency are important attributes of design, such as in aerospace and automotive systems. Additionally, the parallel implementation of the resonant shunt circuit and activity over multiple frequencies, has helped the system adapt to different vibration modes and work scenarios better than a typical single frequency system. It was also shown that airflow significantly impacted the system's performance, suggesting the need to incorporate external dynamic conditions into the model. The figure of the piezoelectric plate in airflow depicted our clear example of how the system worked in a real-world scenario and can be utilized in applications in the future. In this work, our goal has been to lay a foundation for understanding how adaptive, self-sustaining systems that can control vibrations and harness energy at the same time might be developed over time. The multimodal shunt circuit configuration put forth here represents a unique approach to solving the problem of flutter control and energy harvesting, with real possibilities for design within the future of smart structures. Future work will focus on optimizing the system for wider applications and enhanced efficiencies across a wider amplitude of frequencies and varying external conditions.

Acknowledgments

The authors extend their appreciation to the Deanship of Research and Graduate Studies at King Khalid University for funding this work through Large Research Project under grant number RGP.2/94/46. Also, the authors extend their appreciation to Northern Border University, Saudi Arabia, for supporting this work through project number (NBU-CRP-2025-2484).

References

Abad, F. and Rouzegar, J. (2019), "Exact wave propagation analysis of moderately thick levy-type plate with piezoelectric layers using spectral element method", *Thin-Wall. Struct.*, **141**, 319-331. https://doi.org/10.1016/j.tws.2019.04.023

Al-Furjan, M.S.H., Farrokhian, A., Keshtegar, B., Kolahchi, R. and Trung, N.T. (2020), "Higher order nonlocal viscoelastic strain gradient theory for dynamic buckling analysis of carbon nanocones", *Aerosp. Sci. Technol.*, **107**, p. 106259. https://doi.org/10.1016/j.ast.2020.106259

Al-Furjan, M., Xu, M., Farrokhian, A., Jafari, G.S., Shen, X. and Kolahchi, R. (2022), "On wave propagation in piezoelectric-auxetic honeycomb-2d-fgm micro-sandwich beams based on modified couple stress and refined zigzag theories", *Waves Random Complex Media*. https://doi.org/10.1080/17455030.2022.2092235

Al-Osta, M.A., Saidi, H., Tounsi, A., Al-Dulaijan, S., Al-Zahrani, M., Sharif, A. and Tounsi, A. (2021), "Influence of porosity on the hygro-thermo-mechanical bending response of an afg ceramic-metal plates using an integral plate model", *Smart Struct. Syst., Int. J.*, **28**(4), 499-513. https://doi.org/10.12989/sss.2021.28.4.499

Alshenawy, R., Safaei, B., Sahmani, S., Elmoghazy, Y., Al-Alwan, A. and Al Nuwairan, M. (2022), "Buckling mode transition in nonlinear strain gradient-based stability behavior of axial-thermal-electrical loaded fg piezoelectric cylindrical panels at microscale", Engineering Analysis with Boundary Elements, 141, 36-64. https://doi.org/10.1016/j.enganabound.2022.04.022

Alshenawy, R., Sahmani, S., Safaei, B., Elmoghazy, Y., Al-Alwan, A. and Al Nuwairan, M. (2023), "Three-dimensional nonlinear stability analysis of axial-thermal-electrical loaded fg piezoelectric microshells via mkm strain gradient formulations", Applied Mathematics and Computation, 439, 127623. https://doi.org/10.1016/j.amc.2022.127623

Arefi, M. and Bidgoli, E.M.R. (2019), "Electro-elastic displacement and stress analysis of the piezoelectric doubly curved shells resting on winkler's foundation subjected to applied voltage", *Mech. Adv. Mater. Struct.*, **26**(23), 1981-1994. https://doi.org/10.1080/15376494.2018.1430277

Arshid, E., Amir, S. and Loghman, A. (2023a), "On the vibrations of fg gnps-rpn annular plates with piezoelectric/metallic coatings on kerr elastic substrate considering size dependency and surface stress effects", *Acta Mechanica*. https://doi.org/10.1007/s00707-023-03610-6

Arshid, E., Amir, S. and Loghman, A. (2023b), "On the vibrations

of fg gnps-rpn annular plates with piezoelectric/metallic coatings on kerr elastic substrate considering size dependency and surface stress effects", *Acta Mechanica*. https://doi.org/10.1007/s00707-023-03610-6

Asadi, D. and Farsadi, T. (2020), "Active flutter control of thin walled wing-engine system using piezoelectric actuators", Aerospace Science and Technology, 102, 105853. https://doi.org/10.1016/j.ast.2020.105853

Bahrami, A. and Motaei, F. (2025), "One-dimensional phononic crystal fiber for energy harvesting application", *Mech. Adv. Mater. Struct.* https://doi.org/10.1080/15376494.2024.2348600

Bai, J., Liu, G.R., Rabczuk, T., Wang, Y., Feng, X.Q. and Gu, Y. (2024), "A robust radial point interpolation method empowered with neural network solvers (rpim-nns) for nonlinear solid mechanics", *Comput. Methods Appl. Mech. Eng.*, **429**, p. 117159. https://doi.org/10.1016/j.cma.2023.117159

Beni, Z.T. and Beni, Y.T. (2022), "Dynamic stability analysis of size-dependent viscoelastic/piezoelectric nano-beam", *Int. J. Struct. Stabil. Dyn.*, **22**(05), p. 2250050. https://doi.org/10.1142/S0219455422500501

Cao, Y., Weng, M., Mahmoud, M., Elnaggar, A.Y., Zhang, L., El Azab, I.H., Chen, Y., Huang, M., Huang, J. and Sheng, X. (2022), "Flame-retardant and leakage-proof phase change composites based on mxene/polyimide aerogels toward solar thermal energy harvesting", *Adv. Compos. Hybrid Mater.*, **5**(2), 1253-1267. https://doi.org/10.1007/s42114-022-00435-0

Cui, Y., Luo, H., Yang, T., Qin, W. and Jing, X. (2025), "Bio-inspired structures for energy harvesting self-powered sensing and smart monitoring", *Mech. Syst. Signal Process.*, **228**, p. 112459. https://doi.org/10.1016/j.ymssp.2024.112459

De Marqui Jr, C., Vieira, W.G., Erturk, A. and Inman, D.J. (2011), "Modeling and analysis of piezoelectric energy harvesting from aeroelastic vibrations using the doublet-lattice method". https://doi.org/10.1115/SMASIS2011-5204

Dias, J.A. de C., De Marqui Jr, C. and Erturk, A. (2015), "Three-degree-of-freedom hybrid piezoelectric-inductive aeroelastic energy harvester exploiting a control surface", *AIAA J.*, **53**(2), 394-404. https://doi.org/10.2514/1.J053148

Farzam-Rad, S.A., Hassani, B. and Karamodin, A. (2017), "Isogeometric analysis of functionally graded plates using a new quasi-3d shear deformation theory based on physical neutral surface", *Compos. Part B: Eng.*, **108**, 174-189. https://doi.org/10.1016/j.compositesb.2016.09.083

Foroutan, K., Ahmadi, H. and Carrera, E. (2022), "Free vibration analysis of a sandwich cylindrical shell with an fg core based on the cuf", *Smart Struct. Syst., Int. J.*, **30**(2), 121-133. https://doi.org/10.12989/sss.2022.30.2.121

Guo, H., Zhang, C., Fang, H., Rabczuk, T. and Zhuang, X. (2025), "Deep learning to evaluate seismic-induced soil liquefaction and modified transfer learning between various data sources", *Underground Space*. https://doi.org/10.1016/j.undsp.2024.02.001

Hagood, N.W. and Von Flotow, A. (1991), "Damping of structural vibrations with piezoelectric materials and passive electrical networks", *J. Sound Vib.*, **146**(2), 243-268. https://doi.org/10.1016/0022-460X(91)90762-9

Jin, G., Su, Z., Shi, S., Ye, T. and Gao, S. (2014), "Three-dimensional exact solution for the free vibration of arbitrarily thick functionally graded rectangular plates with general boundary conditions", *Compos. Struct.*, **108**, 565-577. https://doi.org/10.1016/j.compstruct.2013.09.061

Kameyama, M. and Makihara, K. (2017), "Piezoelectric energy harvesting from aeroelastic vibration with composite plate wings", *Proceedings of the First International Symposium on Flutter and its Application*, pp. 1-8. https://doi.org/10.1007/978-3-319-65984-4_1

Kheirikhah, M.M., Khalili, S.M.R. and Malekzadeh Fard, K. (2012), "Biaxial buckling analysis of soft-core composite sandwich plates using improved high-order theory", *Eur. J. Mech. - A/Solids*, **31**(1), 54-66. https://doi.org/10.1016/j.euromechsol.2011.07.003

Kong, W., Fu, T. and Rabczuk, T. (2024), "Improvement of broadband low-frequency sound absorption and energy absorbing of arched curve helmholtz resonator with negative poisson's ratio", *Appl. Acoust.*, **221**, p. 110011. https://doi.org/10.1016/j.apacoust.2024.110011

Kulkarni, S. and Kapuria, S. (2008), "Free vibration analysis of composite and sandwich plates using an improved discrete kirchhoff quadrilateral element based on third-order zigzag theory", *Computat. Mech.*, **42**, 803-824. https://doi.org/10.1007/s00466-008-0276-0

Leão, L., De Lima, A., Donadon, M. and Cunha-Filho, A. (2016), "Dynamic and aeroelastic behavior of composite plates with multimode resonant shunted piezoceramics in series", *Compos. Struct.*, **153**, 815-824. https://doi.org/10.1016/j.compstruct.2016.07.003

Li, X., Qin, Y., Yang, D., Deng, J. and Guo, D. (2025), "Investigation of flexural behavior and interfacial performance in cfrp strengthened notched steel beams under adhesive curing using pzt-based wave propagation technique", *Thin-Wall. Struct.*, **208**, p. 112823. https://doi.org/10.1016/j.tws.2024.112823

Lien, I. and Shu, Y. (2012), "Array of piezoelectric energy harvesting by the equivalent impedance approach", *Smart Mater. Struct.*, **21**(8), p. 082001. https://doi.org/10.1088/0964-1726/21/8/082001

Lin, J., Liu, H., Shen, W. and Gu, S. (2024), "Vibration energy harvesting in an fg-cntrc circular microplate with a surface-bonded piezoelectric layer", *Eur. J. Mech.-A/Solids*, **106**, p. 105325. https://doi.org/10.1016/j.euromechsol.2024.105325

Ma, K., Li, Z., Liu, P., Yang, J., Geng, Y., Yang, B. and Guan, X. (2021), "Reliability-constrained throughput optimization of industrial wireless sensor networks with energy harvesting relay", *IEEE Internet Things J.*, **8**(17), 13343-13354. https://doi.org/10.1109/JIOT.2021.3065581

Mangalasseri, A.S., Mahesh, V., Mukunda, S., Ponnusami, S., Harursampath, D. and Tounsi, A. (2023), "Vibration based energy harvesting performance of magnetoelectro-elastic beams reinforced with carbon nanotubes", *Adv. Nano Res., Int. J.*, **14**(1), 27-43. https://doi.org/10.12989/anr.2023.14.1.027

Naranjo-Pérez, J., Infantes, M., Gallegos-Calderón, C.A. and Jiménez-Alonso, J.F. (2024), "The trade-off between structural control and vibration-based energy harvesting: Experimental assessment on a lightweight footbridge", *Mech. Syst. Signal Process.*, **229**, p. 112523. https://doi.org/10.2139/ssrn.4930312

Rabczuk, T., Areias, P. and Belytschko, T. (2007), "A meshfree thin shell method for non-linear dynamic fracture", *Int. J. Numer. Methods Eng.*, **72**(5), 524-548. https://doi.org/10.1002/nme.2013

Rabczuk, T., Ren, H. and Zhuang, X. (2019), "A nonlocal operator method for partial differential equations with application to electromagnetic waveguide problem", *Comput. Mater. Continua*, **59**(1), 31-55. https://doi.org/10.32604/cmc.2019.05668

Ravanbod, M. and Ebrahimi-Nejad, S. (2024), "Perforated auxetic honeycomb booster with reentrant chirality: a new design for high-efficiency piezoelectric energy harvesting", *Mech. Adv. Mater. Struct.*, **31**(27), 9857-9872. https://doi.org/10.1080/15376494.2024.2348601

Sheeraz, M.A., Malik, M.S., Rahman, K., Elahi, H., Khurram, M., Eugeni, M. and Gaudenzi, P. (2022), "Multimodal piezoelectric wind energy harvester for aerospace applications", *Int. J.*

Energy Res., **46**(10), 13698-13710. https://doi.org/10.1002/er.8113

Su, Z., Jin, G. and Ye, T. (2018), "Electro-mechanical vibration characteristics of functionally graded piezoelectric plates with general boundary conditions", *Int. J. Mech. Sci*., **138**, 42-53. https://doi.org/10.1016/j.ijmecsci.2018.01.037

Tiersten, H.F. (2013), *Linear piezoelectric plate vibrations*: *elements of the linear theory of piezoelectricity and the vibrations piezoelectric plates*, Springer. https://doi.org/10.1007/978-1-4615-8278-3

Wang, M., He, J., Zheng, L., Alkhalifah, T. and Marzouki, R. (2025), "Optimizing energy capacity, and vibration control performance of multi-layer smart silicon solar cells using mathematical simulation and deep neural networks", *Aerosp. Sci. Technol*., **159**, p. 109983. https://doi.org/10.1016/j.ast.2025.109983

Wu, S.Y. (1998), "Method for multiple-mode shunt damping of structural vibration using a single PZT transducer", In: *Smart Structures and Materials 1998*: *Passive Damping and Isolation*, Vol. 3327, pp. 159-168. https://doi.org/10.1117/12.316935

Yang, W., Chang, L., Alnowibet, K.A. and El-Meligy, M. (2024), "Enhancing the efficiency and energy capacity of the tri-directional fg nanoplate attached to the piezoelectric patch validated by artificial intelligence", *Aerosp. Sci. Technol*., **155**, p. 109694. https://doi.org/10.1016/j.ast.2024.109694

Zare, R., Najaafi, N., Habibi, M., Ebrahimi, F. and Safarpour, H. (2020), "Influence of imperfection on the smart control frequency characteristics of a cylindrical sensor-actuator gplrc cylindrical shell using a proportional-derivative smart controller", *Smart Struct. Syst*., *Int. J*., **26**(4), 469-480. https://doi.org/10.12989/sss.2020.26.4.469

Zerrouki, R., Hamidi, A., Tlidji, Y., Karas, A., Zidour, M. and Tounsi, A. (2022), "Free vibration responses of nonlinear fg-cnt distribution in a polymer matrix", *Smart Struct. Syst*., *Int. J*., **30**(2), 135-143. https://doi.org/10.12989/sss.2022.30.2.135